5ICEGE
5th International Conference on Earthquake Geotechnical Engineering
January 2011, 10-13 | Santiago, Chile
Paper No. NIOKT

NUMERICAL INVESTIGATION OF SITE EFFECTS AT AEGION, GREECE

Olga-Joan KTENIDOU [1], Francisco. J. CHÁVEZ-GARCÍA[2], Dimitris RAPTAKIS[3] and Kyriazis PITILAKIS[4]

ABSTRACT

This paper aims at studying the effects of surface and subsurface topography on seismic response through 2D numerical analysis with the finite difference method. The city of Aegion is studied because it is a highly seismic region that combines several geomorphological features: surface topography (with the Aegion fault dividing it in two levels) and a sedimentary basin with complex non-horizontal layering at its northern part, towards the Gulf. The morphology, geology, and dynamic soil parameters are known through prior investigations which resulted in a detailed 2D cross-section perpendicular to the fault, comprising both levels of the city. This section is modeled and 2D dynamic analysis is performed using two finite difference schemes with incident SH and SV waves. The effect of material damping is included. The numerical results along the surface of the model are compared with 1D analysis results, revealing higher spectral amplification around the fundamental frequency for 2D compared to 1D analysis. This is due to the diffracted surface waves generated at the lateral discontinuities and soil interfaces, which also cause higher amplification for SH than for SV waves in the basin. We focus on engineering aspects of the ground motion such as peak motion values and topographic amplification. Ground motion assumes higher values near the slope and in the basin near each outcropping soil interface. Topographic amplification is compared with the values predicted by codes and suggestions are made so that they may suffice.

Keywords: 2D dynamic analysis, small-strain damping, basin, topography, amplification, Gulf of Corinth

INTRODUCTION

Local site conditions can influence the characteristics of strong ground motion in various ways, which are collectively referred to as site effects. These are related to the thickness and impedance contrast between soil layers, the surface topography, lateral discontinuities, basin edges, inclined interfaces, soil inhomogeneities, etc. While soil layer effects can be predicted rather straightforwardly, topography and basin edge effects present more complications, since they are tied to two-dimensional phenomena such as focusing and defocusing of seismic energy, interference of direct and diffracted wave fields, and generation of surface waves leading to complex wave fields (Bard, 1999).

In this study, a site is chosen which combines several of the aforementioned geomorphological features. It is modeled based on existing knowledge of the geometry and properties of the geological structures. The

[1] Dr, Department of Civil Engineering, Aristotle University Thessaloniki, e-mail: ktenidou@civil.auth.gr.
[2] Professor, Instituto de Ingeniería, Universidad Nacional Autónoma de México, e-mail: paco@pumas.iingen.unam.mx.
[3] Assistant Professor, Department of Civil Engineering, Aristotle University Thessaloniki, e-mail: raptakis@civil.auth.gr.
[4] Professor, Department of Civil Engineering, Aristotle University Thessaloniki, e-mail: kpitilak@civil.auth.gr.

numerical analysis results are used to highlight the influence of the site's features, namely topography and basin effects from complex non-horizontal layering, on certain aspects of site response which present particular engineering interest.

AVAILABLE DATA

The area studied was the city of Aegion, which lies on the southern part of the Gulf of Corinth, Greece (Fig. 1), a highly seismic area comprising many WNW-trending, north-dipping active normal faults. The city has been struck by significant earthquakes in the past, the strongest re-cent one being that of June 15, 1995 (Ms=6.2). The chosen region is marked on the one hand by its characteristic surface topography, given that it is traversed by the Aegion fault, whose escarpment of roughly 90 m divides the city into two levels: the lower Northern part lying on the hanging wall and the upper Southern part lying on the foot wall (Fig. 1a). On the other hand, another characteristic feature of the site relates to the loose soft deposits present downhill, which form an open basin whose depth increases along with the sea depth.

After a series of field and laboratory tests, as well as borehole logging, geophysical prospecting and microtremor measurements, Apostolidis et al. (2005) modeled the complex geology of the site in detail and estimated the geotechnical and dynamic soil properties to a satisfactory degree. The model proposed by them can be seen in Fig. 1. At the lower part of the city, very near the coast, the soil profile consists of soft loose marine materials (with thickness up to 200 m) overlying hard conglomerate. At the upper part of the city, the soil profile consists of a thin layer of deposits overlying the stiff conglomerate.

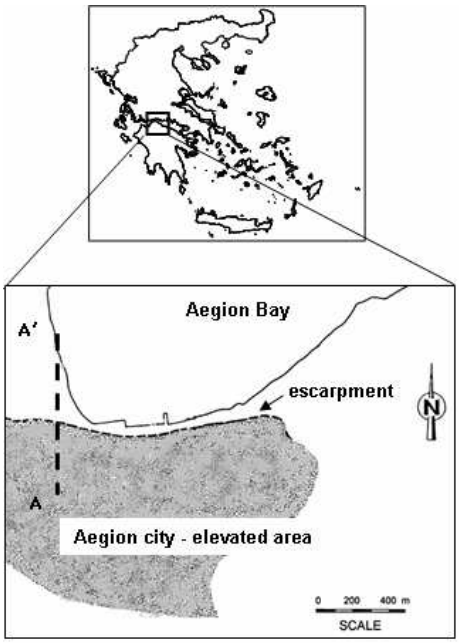

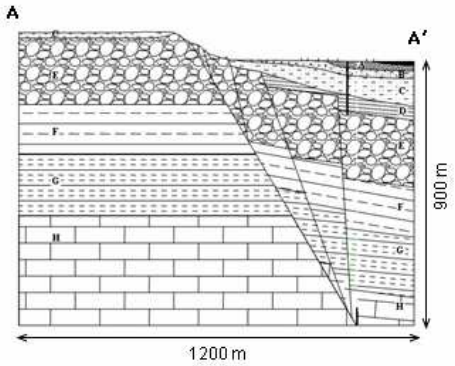

Formation	Description	Vs (m/sec)
A	Soft marine deposits consisting of sandy silt, silt, silt and clay (SM-ML-CL)	150-200
B	Soft sediments consisting of clayey silt, sandy clay, silty clay with few gravels (SC-ML-CL)	220-310
C	Hard deposits consisting of clayey silt, sandy clay, silty clay, with few gravels (SC-ML-CL)	370-490
D	Very hard deposits consisting of sandy gravels, sandy clay with few gravels (GW-GP-CL), NSPT	490-590
E	Stiff conglomerate with RQD 20% - 30%	800-1200
F	Marine clay	>800
G	Radiolarits and limestones	>1000
H	Limestone	>1200

Figure 1. Left: Location of site under study and map of the city of Aegion indicating fault escarpment, elevation differences and A-A' cross-section (adapted from Athanasopoulos et al. 1999). Right: Geotechnical model of the cross-section crossing the fault (Apostolidis et al. 2005).

SIMULATION

The 2D numerical modelling was based on the geotechnical model of Apostolidis et al. (2005) shown in Fig. 1. One alteration made to that for the purposes of the numerical analysis was that the deposit-conglomerate interface (D-E) was smoothed so as not to introduce angular interfaces which are uncertain in the first place and may generate artificial complications. Another alteration was that no more interfaces were considered beneath the conglomerate-deposit interface, since their actual location is dubious and only assumptions can be made as to the deeper formations' dynamic properties. Besides, the greatest impedance contrast is that between the soils and the conglomerate. The model of Apostolidis et al. (2006) has a width of only 1.2 km, which was not enough to avoid artificial reflections at the right boundary. For this reason, a third modification was required: extending it laterally to the North. The inclined layers were extended 300 m following their slope and then they were changed to flat layers until the right boundary of the model. Thus the part from x=1500 m to x=2000 m was used as a horizontally layered 1D extension of the model in which artificial reflections were dissipated. The depth of the base was also chosen to avoid artificial motion in the grid. The geometry and soil properties of the model used are shown in Fig. 2.

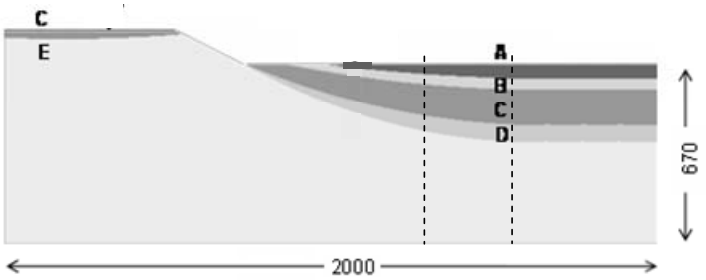

Figure 2. Geometry of the numerical model used. The vertical lines indicate distances x=1200 m, where the model of Apostolidis et al (2006) ends, and x=1500m, where the layers are extended horizontally towards the North.

Two different 2D finite difference (2DFD) schemes were implemented for the dynamic numerical analysis, one using vertically incident SV motion and allowing for P-SV interaction and one using plane SH vertically incident waves. The first code was FLAC 2D v. 4 (ITASCA, 2002 & 2005) and the second one was SH11, the scheme introduced by Moczo (1989) and Moczo & Bard (1993). For both schemes the discretisation was performed so as to allow frequencies up to 10 Hz to propagate without distortion through the grids. Though the model geometry is exactly the same for the two codes, the number and size of grid zones is different.

The linear elastic model was used. Based on the ranges given by Apostolidis et al. (2006), a Vs value was chosen for each material modeled. The soil densities were chosen based on laboratory tests. No water table was defined. The Poisson ratio was assumed to be 0.3 for soils and 0.2 for the conglomerate.

Material damping based on available G-γ-D curves was introduced into the calculations to account for small-strain energy dissipation. Damping is simulated in different ways in the two codes. This is one of the reasons for which analyses were first performed using zero damping to compare the two codes. Then, material damping was introduced into the calculations to account for small-strain energy dissipation. In FLAC2D Rayleigh damping is used. We choose an average value ξ for each soil layer based on prior kno-

wledge from dynamic soil tests (Pitilakis et al., 2004). These damping values are shown in Table 1 and they were centred around a central frequency of f_{min}=2.4 Hz. This provides relatively frequency-independent damping for the frequency range we are most interested in from 1 to 6 Hz, which includes most of the model's natural frequencies (since it is defined by the downhill and uphill resonant frequencies respectively) as well as the predominant input frequencies. In the case of SH11, damping is simulated through a rational approximation of the frequency-dependent viscoelastic modulus Q introduced by Emmerich and Korn (1987) for time-domain calculations. This method is based on the rheological model of the generalised Maxwell body. Three logarithmically equidistant relaxation frequencies are chosen for all materials: 0.1, 1.0 and 10.0 Hz. Since the numerical damping is roughly constant within this range, the quality factor is derived from the damping values (ξ) based on the relation Q-1=2ξ, which is valid for weak to moderate damping. The Q values are also shown in Table 1.

Table 1. Mechanical and dynamic soil properties of the materials modeled.

Soil type	d [kN/m^2]	Poisson's v	Vs [m/s]	ξ (SV)	Q=1/2 ξ (SH)
A	18.5	0.3	180	1.8%	28
B	19.5	0.3	265	2.5%	20
C	19.5	0.3	440	2.6%	19
D	20.0	0.3	540	2.0%	25
E	21.0	0.2	1000	0.5%	100

The input motion time-history was the same in both cases: a displacement pulse given by the Gabor wavelet, which has been used by Moczo (1989) and is described by equation 1:

$$S(t) = \exp\left(-\frac{\omega\cdot(t-t_s)}{\gamma}\right)^2 \cdot \cos\left(\omega\cdot(t-t_s)+\psi\right) \quad (1)$$

where $\omega = 2\pi\cdot f_p$, $t_s = 0.45\cdot\gamma/f_p$, f_p is the predominant frequency, and the pulse is defined in the interval [0. 2]. In this case, we considered the parameters used by Makra et al. (2001), namely: γ=1.5, f_p=4 Hz, ψ=0.4, and t_s=0.169 s. This allows for a pulse whose amplitude spectrum is almost flat over most of the frequency range we are interested in, which is roughly between 0.1-10 Hz (Fig. 3).

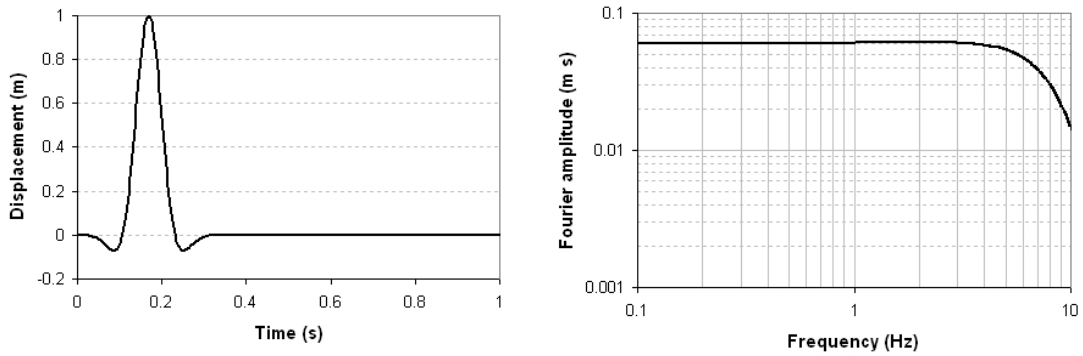

Figure 3. The time-history and Fourier amplitude spectrum of the Gabor wavelet used as seismic excitation in calculations.

TIME-DOMAIN RESULTS

Seismic sections

One of the techniques usually implemented for visualising results in the time domain is the seismic section. In Fig. 4, the results are displacement time histories taken every 10-12 m along the profile. All components of motion are shown: the transverse (perpendicular to the cross-section, SH waves), the radial (parallel to the section, P-SV interaction) and the vertical (P-SV interaction due to the non-horizontal boundaries). Following arrival of all direct and reflected S waves (around 1 s uphill and 1.5 s downhill), laterally propagating surface waves are clearly seen. The effect of the relief in the overall response of the actual site is weak. The existence of layering both uphill and downhill gives rise to reflected S waves and - in later phases- diffracted surface waves that increase the duration of shaking significantly. An important feature of the site's response is the fundamental-mode surface wave (Rayleigh for the SV analysis and Love for the SH analysis) generated near the edge of the basin and propagating outwards at roughly 180 m/s, which is the shear wave velocity of the topmost layer, meaning the wave is guided by it. The phase velocity of the fundamental mode is marked in the figure on one of the plots. SH motion (out-of-plane motion is parallel to the basin edge) is stronger than SV motion (in-plane motion, perpendicular to the basin), i.e. Love waves are stronger than Rayleigh waves. The stronger amplification of the transverse component in Aegion was verified also by some instrumental results of Ktenidou (2010), while it is also mentioned in the literature by Jongmans and Campillo (1993) and Chávez-García and Faccioli (2000).

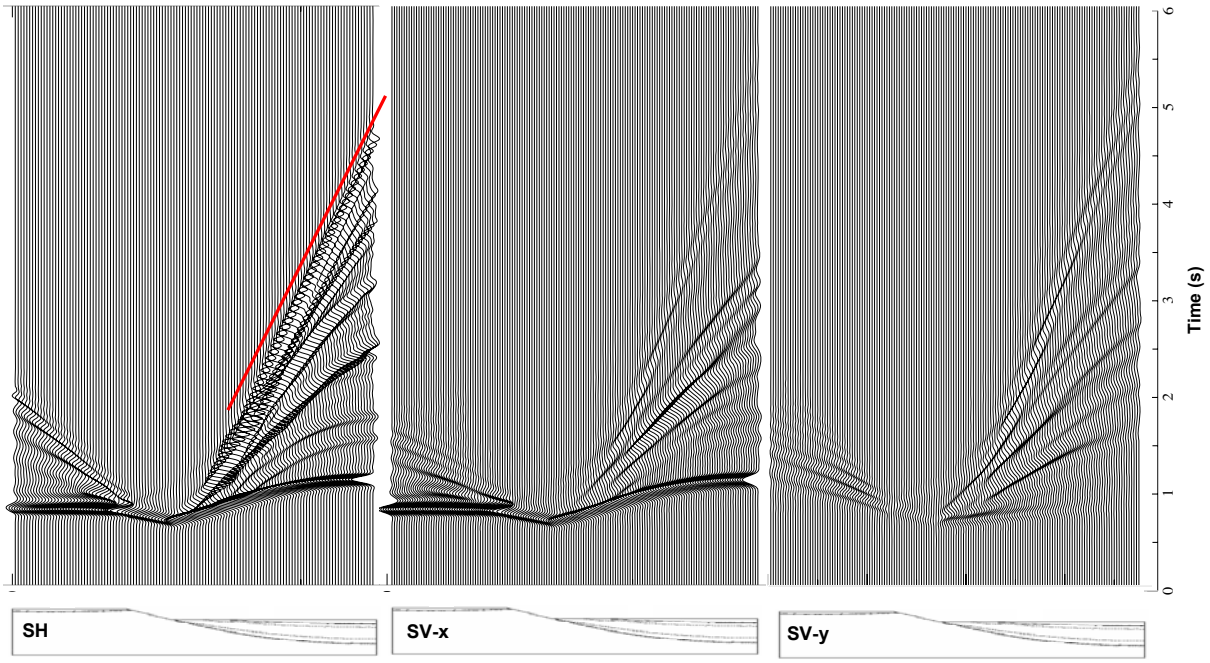

Figure 4. Displacement time-histories along the model surface for the transverse (left), radial (centre) and vertical (right) component, as calculated through 2D SH and SV analyses including damping.

Peak values

Peak ground motion is of interest when considering site effects from an engineering point of view, because in design it is often a single value prescribed by codes that is used to account for site amplification. Even though a single value cannot reflect the complex, frequency-dependent phenomena that take place when surface and lateral subsurface discontinuities are present, it is interesting to observe the variation of this peak value across our profile. Based on Fig. 4, we plot the maximum value of each trace in the time domain across the length of the cross-section. This yields Fig. 5, in which values are dimensionless because they correspond to unit-amplitude input. Near the crest, motion is amplified in a rather simple pattern due to topography effects. However, in the basin, the amplification pattern becomes more complex and the amplification level increases due to the presence of the various layer interfaces. We observe a step-like increase in amplitude as the basin deepens up to a distance of 400m from the toe, with the steps relating to the location of outcropping interfaces of the model. The vertical component generated from the P-SV interaction is not negligible, since its amplitude is comparable to the amplitude of the input.

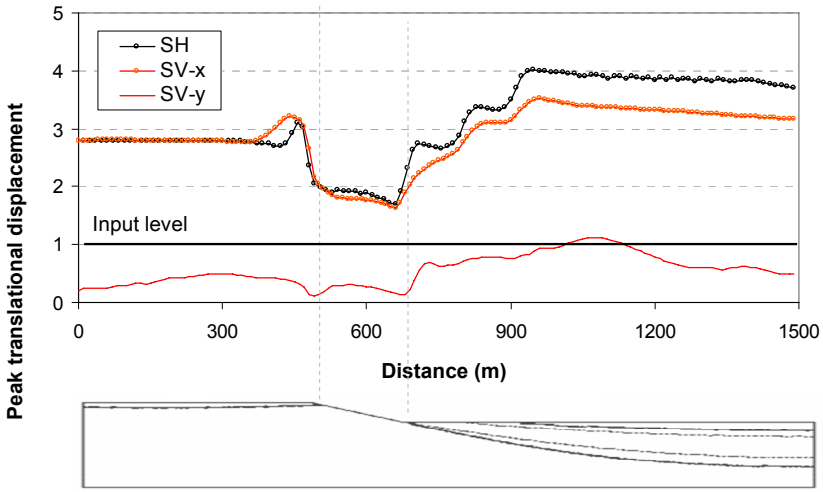

Figure 5. Peak displacement values for the radial (SV-x), transverse (SH) and vertical (SV-y) component along the model surface (for unit input), calculated through 2D SV and SH numerical analyses including damping.

FREQUENCY-DOMAIN RESULTS

Transfer functions

The horizontal synthetics were divided in the frequency domain by the input motion to compute transfer functions. In Fig. 6 these are plotted as contours of equal amplification for frequencies from 0.1 to 10 Hz. Uphill, we observe amplification for frequencies 4-5 Hz, which correspond to the 1D resonant frequency of the stiff deposits over the conglomerate. Downhill, the fundamental amplification peak is observed beneath 1 Hz at large distances from the crest where the deposits become very thick. These frequencies were also validated instrumentally from records available both uphill and downhill (Ktenidou, 2010). Observing higher modes, the succession of peaks in the transfer functions does not correspond exactly to the 1D resonance pattern. The spacing of the peaks in frequency is denser than the $(2n+1)\cdot f_o$ rule. This cannot be due only to vertically propagating body waves and is probably also related to lateral effects. As was seen in the time-domain results as well, SH amplification is stronger than SV motion, again implying stronger Love waves than Rayleigh waves.

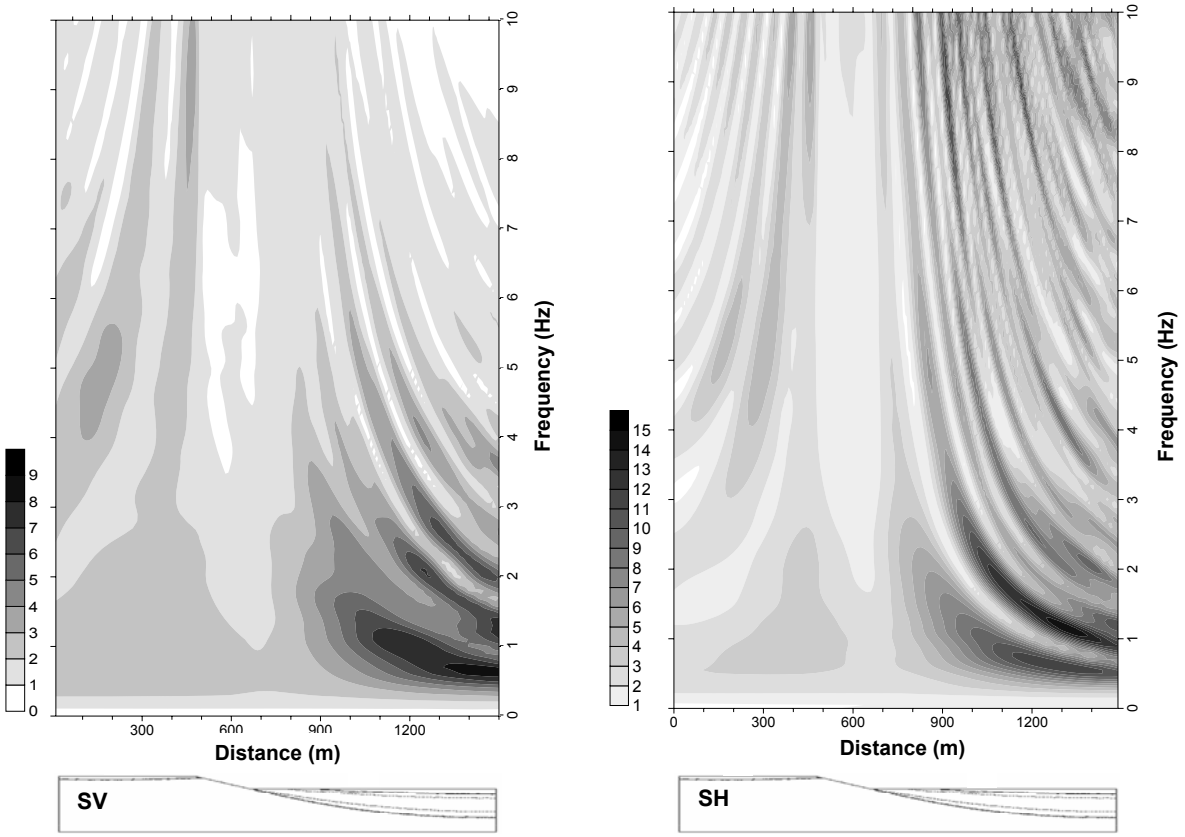

Figure 6. Transfer functions for the SV analyses (left) and SH analysis (right) including damping.

Comparison with 1D analyses

We compare our 2D results with some 1D results calculated at various locations across the model. 1D profiles were extracted from the 2D model at 50 m intervals (except along the fault escarpment, which consists entirely of conglomerate). 1D analyses were performed using the reflectivity method (Kennet, 1983). Vertical incidence of SV waves was assumed and calculations were made in the frequency domain. This requires for each layer its thickness, mass density, seismic wave velocity (Vs), and quality factor (Qs). The quality factor was computed from the minimum D values of the available G-γ-D curves. Fig. 7 shows the spectral amplification at the resonant frequency at each location, as computed through the 2D and 1D analyses. Clearly, spectral amplification is inadequately predicted by 1D analysis both uphill and downhill. Topographic amplification behind the crest reaches 3 (for SV) and 5 (for SH) rather than 2, which is the 1D prediction. In the basin the discrepancies between 1D and 2D computations are even greater. 1D soil effects cause amplification up to 3, while when 2D effects such as lateral propagation of surface waves are considered then amplification reaches 8 (SV) to 11 (SH). Again we see that 2D amplification is greater in the SH case than in the SV case both uphill and downhill. Uphill, the zone of topographic influence from the crest is also larger in the SH case.

TOPOGRAPHIC AMPLIFICATION AND DESIGN CODES

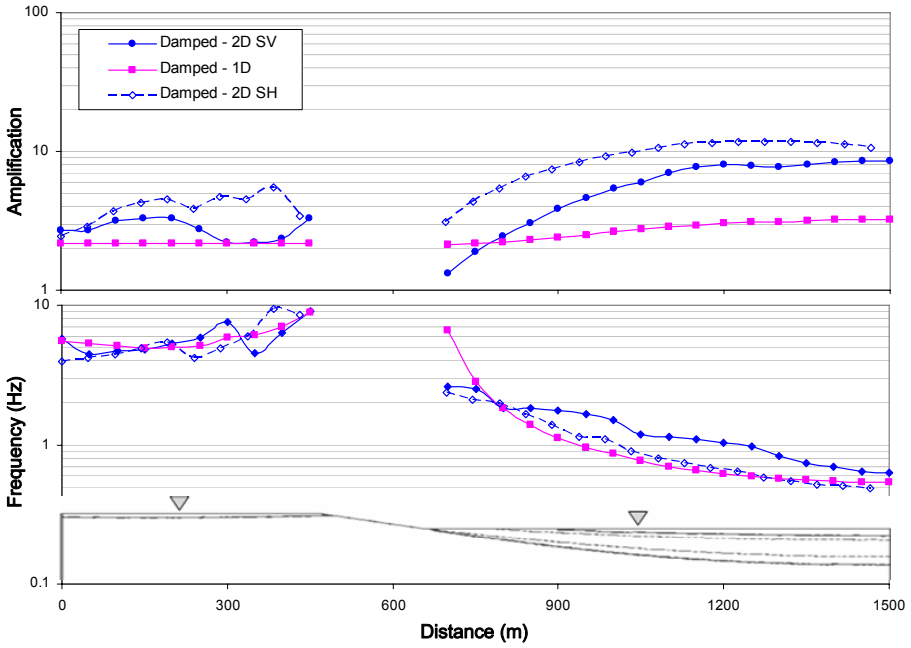

Figure 7. Comparison of 2D (SV and SH wave incidence) and 1D spectral amplification at the resonant frequency. Bottom: resonant frequency. Top: corresponding amplification level.

As no design codes account for basin-edge effects, we focus on code predictions for topographic amplification and compare them with the amplification we computed behind the crest. Topography effects are taken into account in two design codes, the French AFPS90 and EC 8 (AFPS, 1995; ECN, 2003):

- The French recommendations AFPS define a coefficient that is frequency independent and has a maximum value of 1.40. The coefficient is defined depending on the slope inclination (I) and its difference with the slope of the ground behind the crest (i). It is applied over a length 'b' from the crest of the slope and is linearly reduced to 1.0 over transition lengths 'a' and 'c' in front of and behind the crest, respectively (see Bard, 1999, for an illustration and details). The conditions under which the topographic effect is taken into account are the following: slope height H>10m, slope inclination I>22° and ground inclination behind the slope i< 0.33I.
- Eurocode 8 also defines an amplification factor (ST) that is frequency independent to be used for important structures. The minimum slope inclination taken into account is 15° and the minimum height considered is H=30m. The factor takes values up to 1.40. The length behind the crest over which it is applied is not defined. It is mentioned that for isolated cliffs and slopes, a value of ST>1.2 should be used for sites "near" the top edge.

Because of the soft surface layer present uphill at Aegion, soil effects render it difficult to quantify the effect of the relief. For this reason the peak ground motion in the vicinity of the crest (Fig. 5) is normalised by the peak ground motion at the far field in order to be compared with codes (Fig. 8). For the P-SV numerical scheme, amplification in the time domain extends to a distance of 100 m behind the crest and reaches up to 17%, while for the SH scheme this distance is only 40 m and the increase is not higher than 12%. Though this difference is not great, it is in agreement with the observation mentioned by Geli et al. (1988) and Bard (1999) that the motion perpendicular to the ridge axis is often larger.

Fig. 8 also shows the comparison of the results with the two codes. Aegion's relatively mild relief corresponds to topographic amplification values of just 1.07 and 1.2 for AFPS and EC8 respectively, with 1.4 being the maximum value either code allows. AFPS gives precise rules to define the factor for topographic amplification as a function of distance from the crest. We apply them and find that the AFPS envelope is insufficient for predicting the results of the 2D computations, both in terms of amplification level and zone of influence. This is especially the case for SV wave incidence. In contrast, EC8 leaves it to the engineer to interpret what distance is considered 'near' the crest and at what distance the effect disappears. Here, two distances are chosen: the distance according to AFPS (b_{AFPS}=10 m) and a distance equal to half the height of the slope (H/2=45 m). The respective envelopes are plotted following the slope of the AFPS envelope (marked in the figure as lines 1 and 2 respectively for the two distances). EC8 predicts successfully the amplification level for the SH analysis and need only be applied over a short distance from the crest: up to 10 m followed by a linear decrease of amplitude to zero at 75 m. For SV analyses, the EC8 envelope needs to be extended to 45 m and followed by a linear decrease of amplitudes to zero at 110 m. We may note that EC8 allows for a 25% increase in the topographic factor if there is a soft surface layer is present with thickness larger than 5 m (the properties of the layer are not defined); if we consider the soil layer uphill as soft then the factor becomes 1.5.

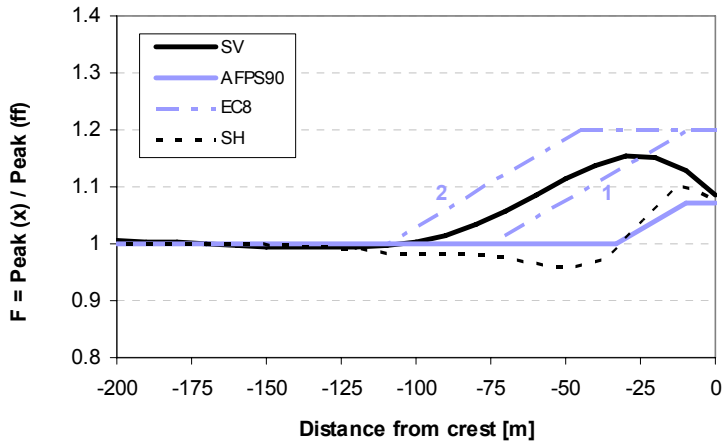

Figure 8. Peak horizontal displacement in the vicinity of the crest, normalised by the amplitude at the uphill far field, calculated by SV and SH analysis including damping. Comparison with AFPS envelope and with two indicative EC8 envelopes for different influence zones (1: b_{AFPS}=10 m, 2: H/2=45 m).

CONCLUSIONS

The complex site of Aegion is chosen because its geomorphological features include surface topography and a basin with non-horizontal layering. The site is modelled based on existing knowledge of the geometry and properties of its geological structures. Small-strain anelastic material attenuation is taken into account. We use two finite difference schemes for dynamic analysis, one to model SH motion and one to model P-SV motion. 1D analyses prove inadequate in predicting amplification behind the crest and in the basin. The existence of layering uphill and especially of the basin downhill gives rise to complex 2D phenomena and amplification patterns due to reflected body waves and diffracted surface waves. These increase the duration of shaking significantly; they also amplify peak time-domain amplitude as well as the resonant spectral amplification. SH amplification is stronger than SV amplification in the basin. This corresponds to the transverse component being stronger than the radial one and has been mentioned before in instrumental and computational studies. Uphill, topographic amplification in the time domain is

observed up to 100 m from the crest according to the P-SV scheme and 40 m for the SH scheme. The respective maximum amplification factors are 1.17 and 1.12, compared with the respective 1D case. The AFPS provisions do not successfully envelop the numerical results (particularly for SV analysis), while EC8 could achieve that if applied to an appropriate distance from the crest (equal to half the slope height).

AKNOWLEDGEMENTS

FJCG thanks Coordinación de la Investigación Científica, UNAM, for support.

REFERENCES

AFPS (Association Française du Génie Parasismique) (1995). Guidelines for seismic microzonation studies. AFPS/DRM, 45 pp.

Apostolidis P., Raptakis D, Pandi K., Manakou M., and Pitilakis K. (2006). "Definition of subsoil structure and preliminary ground response in Aigion city (Greece) using microtremor and earthquakes", Soil Dyn. Earthq. Eng. Vol. 26, pp. 922 - 940.

Bard P.-Y. (1999) "Local effects on strong ground motion: Physical basis and estimation methods in view of microzoning studies". Proc. of Advanced Study Course in 'Seismotectonic and Microzonation techniques in Earthquake engineering, Kefalonia, Greece.

CEN (European Committee for Standardisation) (2003). Eurocode 8: Design of structures for earthquake resistance. Part 5: Foundations, retaining structures and geotechnical aspects, Draft No. 5 (prEN 1998-5). Brussels, Belgium.

Chávez-García F.J., and Faccioli E. (2000). "Complex site effects and building codes: Making the leap", J. Seismology Vol. 4, pp. 23-40.

Emmerich, H. and M. Korn (1987). "Incorporation of attenuation into time-domain computations of seismic wave fields", Geophysics Vol. 52, pp. 1252-1264.

Geli L., Bard P.Y., and Jullien B. (1988). "The effect of topography on earthquake ground motion: a review and new results", Bull. Seism. Soc. Am. Vol. 78, pp. 42-63.

ITASCA (2002). FLAC – Fast Lagrangian Analysis of Continua – Version 4.0. User's Guide, Itasca Consulting Group, Minneapolis, USA.

ITASCA (2005). FLAC – Fast Lagrangian Analysis of Continua – Version 5.0. User's Guide, Itasca Consulting Group, Minneapolis, USA.

Jongmans D., and Campillo M. (1993). "The response of the Ubaye Valley (France) for incident SH and SV waves: Comparison between measurements and modelling", Bull. Seismol. Soc. Am. Vol. 83, pp. 907-924.

Kennet, B.L.N. (1983). "Seismic wave propagation in stratified media". Cambridge University Press.

Ktenidou, O.-J. (2010). "Theoretical and instrumental study of site and topographic effects on strong ground motion in Aegion". PhD thesis, AUTh, Greece.

Makra K, Raptakis D, Chávez-García FJ, Pitilakis K. (2001). "Site effects and design provisions: the case of Euroseistest", Pure Appl. Geophys. Vol. 58, pp. 2349–67.

Moczo P. (1989). "Finite difference technique for SH waves in 2-D media using irregular grids: application to the seismic response problem", Geophys. J. Int. Vol. 99, pp. 321–9.

Moczo P, Bard P-Y. (1993). "Wave diffraction, amplification and differential motion near strong lateral discontinuities", Bull. Seism. Soc. Am. Vol. 83, pp. 85–106.

Pitilakis K., Makropoulos K., Bernard P., Lemeiile F., Lyon-Caen H., Berge-Thierry C., Tika Th., Manakou M., Diagourtas D., Raptakis D., Kallioglou P., Makra K., Pitilakis D., Bonilla F. (2004). "The Corinth Gulf Soft Soil Array (CORSSA) to study site effects/Le réseau en sols meubles (CORSSA) du Golfe de Corinthe pour l'étude des effets de site", C. R. Geoscience 336, pp. 353- 365.